Uptake of SO₂ by Polycrystalline Water Ice

Thomas Huthwelker,*,§,[1] Dennis Lamb,† Marcia Baker,‡ Brian Swanson,‡ and Thomas Peter*

Laboratorium für Atmosphärenphysik der ETH (LAPETH), CH-8093 Zürich, Switzerland; †Meteorology Department, 503 Walker Building, The Pennsylvania State University, University Park, Pennsylvania 16802; ‡Department of Earth and Space Science, University of Washington, Seattle, Washington 98195-1650; and §Physics Department, University at Albany (SUNY), 1400 Washington Avenue, Albany, New York 12222

We have investigated two previous experimental studies (Clapsaddle and Lamb, 1989; Conklin *et al.* 1989) of SO₂ uptake into polycrystalline ice the results of which seem to conflict. Both studies employed porous packed beds prepared by freezing 200-μm-diameter water drops in liquid nitrogen followed by aging. In the absence of oxidation, uptake was measured via frontal chromatography at various temperatures between -60 and $-1°$C, with SO₂ mixing ratios between 15 and 100 ppb. The experiments differed primarily in the ice surface areas and exposure times, yielding purportedly equilibrium surface coverages that differed by more than a factor of 50. The uptake increased with temperature and with a less than linear dependence on partial pressure. Our comparison shows that a kinetic model is needed for interpretation partly explaining the apparent discrepancy between the two investigated uptake experiments. The uptake rates, its amount, and its temperature dependence suggest that SO₂ dissociates and diffuses into an internal reservoir for example comprised of veins and nodes, but not into a surface layer as previously hypothesized. Whereas slow diffusion may remain undetected during the relatively short time scales of laboratory experiments, it may dominate trace gas uptake by natural ice. We suggest that dry deposition schemes of SO₂ onto snowpacks in climate models should include the kinetics of uptake and account for the temperature and pressure dependencies found in the laboratory studies reviewed here. © 2001 Academic Press

Key Words: ice, SO₂ uptake; quasi-liquid layer; veins.

1. INTRODUCTION

Despite 150 years of research into the physics of water ice (for review see (3–5)) considerable debate still revolves around the nature of the ice surface and its interaction with a gaseous environment (6–10). Recent studies (e.g., (11–17)) have variously invoked surface adsorption, absorption into a surface-melted or "quasi-liquid" layer (QLL), bulk diffusion into the ice lattice, and segregation into inclusions or grain boundaries as possible uptake mechanisms. Under some circumstances, especially at relatively high partial pressures, the uptake may lead to significant melting point depression, to the formation of hydrates, and to environmentally important chemical reactions (e.g., (18, 19)).

Natural ice occurs in a wide range of forms and is invariably exposed to many different chemical species (see Hobbs, 1974 (5), Chap. 10, or Petrenko and Whitworth, 1999 (4), Chap. 12, for overviews). Ice in the atmosphere often forms within clouds as single crystals that aggregate and fall to the surface as snow, but polycrystals also arise in clouds during the freezing of supercooled water drops, leading to graupel and/or hail. Snow and ice on the surface, such as the seasonal snowpack, glaciers, and lake or sea ice, are typically polycrystalline in nature. Polycrystalline ice is characterized by numerous ice–ice boundaries that separate the individual "grains" of monocrystalline ice from each other. The network of "grain boundaries" (surfaces between two grains), "veins" (the linear intersections of grain boundaries), and "nodes" (the junctions of veins) in a polycrystalline system provides a complex matrix within which environmental chemicals may interact (20–23).

The rates and total amount of the gas taken up by any given ice sample depend on a number of parameters, most notably the temperature and the partial pressure of the gas, and the surface state of the ice, as well as its polycrystallinity and bulk morphology (24, 25). Temperature plays a particularly important role in controlling the rate of gaseous exchange across the solid–vapor interface, as well as the magnitude of the overall uptake. The temperature dependence of the hypothesized liquid-like properties of the ice surface (26–32), for instance, has been invoked to explain various experimental data and to model environmental effects (1, 6, 17, 33, 34). Because the thickness of the disordered surface region of ice increases strongly as the temperature approaches the melting point, one might reasonably expect the equilibrium uptake to increase with temperature, in opposition to classical adsorption behavior. Such anomalous behavior is clearly seen in the packed ice bed experiments of Clapsaddle and Lamb (1) and Conklin *et al.* (2), but we will see later that simple interpretations based on absorption into a QLL may not be fully justified.

When in contact with highly water-soluble acidic vapors, like HCl or HNO₃, ice may melt even under quite low gas partial pressures (16, 19, 35). For example, melting is known to occur at HCl partial pressures of 8×10^{-3} Pa near temperatures of $-70°$C (34). Such melting can influence both the uptake amount and the kinetics of the uptake process (for example, see (17)). On the other hand, the low solubility of a gas like SO₂ leads
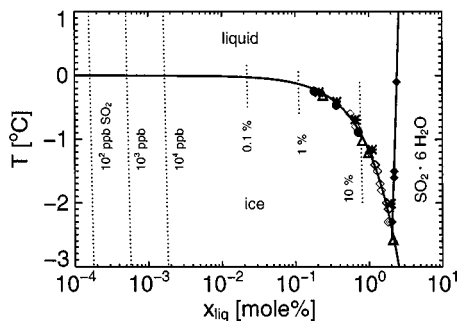
---

[1] To whom correspondence should be addressed. E-mail: huthw@atmos.umnw.ethz.ch.

FIG. 1. Phase diagram of the SO_2/ice system plotted as temperature T versus SO_2 mole fraction expressed as % in the solution, calculated after Gmelin (62). Solid curves represent the coexistence temperature of the aqueous SO_2 solution with ice and with the $SO_2 \cdot 6H_2O$ hydrate, respectively. Dotted lines show the composition/temperature dependence for constant SO_2 mixing ratios (in ppb = 10^{-9}, % = 10^{-2}) at normal pressure. Various symbols indicate measurements of the melting point depression for solutions of different compositions, as given in (62).

to melting point depressions that are negligible at typical atmospheric mixing ratios (which range from several ppt in rural areas to occasionally over 100 ppb in highly polluted regions (36)). Consideration of the bulk SO_2–water phase diagram (Fig. 1) shows that a mixing ratio of 0.1–1% (corresponding to an SO_2 partial pressure of 10^2–10^3 Pa) is necessary to reduce the melting point of ice by 0.1°C. Given the modest Henry's law constant of SO_2 in water (e.g., (37)), such a partial pressure corresponds to an aqueous SO_2 concentration of about 0.1 mol%. The formation of other solid phases, such as the $SO_2 \cdot 6H_2O$ hydrate, becomes possible only once the SO_2 partial pressures become greater than about 3×10^4 Pa. Therefore, SO_2 partial pressures as they occur in the natural environment and as they were used in the laboratory as discussed below lead neither to melting of ice nor to the formation of new phases.

As a consequence of the importance of SO_2 chemistry in the environment, particular attention has been paid in recent years to SO_2 uptake by water ice. Several laboratory experiments have investigated this phenomenon using diverse experimental techniques over a range of thermodynamic conditions (1, 2, 33, 38–43). For example, Mitra *et al.* (41) measured uptake onto dendritic snowflakes and Valdez *et al.* (39) investigated uptake into growing ice, while Conklin *et al.* (2, 33) and Clapsaddle and Lamb (1) studied the uptake of SO_2 into packed beds of polycrystalline ice. Both direct comparison of experimental results and identification of the relevant physical/chemical mechanisms are made difficult in the absence of a verifiable process model.

In this paper we focus attention on the two sets of packed-bed experiments by Conklin *et al.* (2) and by Clapsaddle and Lamb (1) (referred to hereafter as C and CL, respectively), because the preparation of the ice samples, the partial pressures, the temperatures, and the experimental setups were similar and well controlled. Despite these similarities, the empirical findings and conclusions of the authors differed substantially. The goal of this paper is therefore to compare various models of gas uptake with the results obtained from these two experiments in

order to infer the likely uptake reservoir and to see if a common mechanism of uptake exists. After a brief review of the C and CL packed-bed experiments and their original findings, we apply theoretical expressions (derived in the Appendix) for time-dependent uptake to the laboratory data. The discussion of the results leads us to conclude that the common mechanism was likely to have been diffusion into a temperature-dependent reservoir, most likely the veins, nodes, or grain boundaries of the polycrystalline ice. Finally, we offer ways to apply this new model of the uptake process to interactions of trace gases with ice in the natural environment.

2. METHODS

2.1. The Packed-Bed Experiments Reviewed

Both C and CL investigated the uptake of gaseous SO_2 into packed ice beds by frontal chromatography using practically identical experimental setups. In both sets of experiments a gaseous mixture of prehumidified air and SO_2 with a constant input partial pressure p_{in} was passed through the packed bed of ice held at a chosen temperature T. The data were presented in terms of breakthrough curves, i.e., graphs of measured SO_2 partial pressure $p_{out}(t)$ leaving the ice sample at time t after the gas inflow began. Each experiment ran for a time t_{end} (the SO_2–ice exposure time), defined roughly as the point at which $p_{out}(t_{end}) = p_{in}$ within experimental accuracy. (We will show below that equilibrium was probably not reached in either the C or CL experiments.) At $t = t_{end} \approx 1$ to 6 h, C assumed that the uptake was finished and that the ice was saturated. The uptake amount in the experiments of C was determined by chemical analysis (ion chromatography) of the melted ice sample. By contrast, the CL experiments had typical SO_2–ice exposure times of 1 to 2 days, and even then it appears that saturation was not reached. Therefore, CL (who determined the uptake by subtracting the up- and downstream concentrations measured with a flame-photometric sulfur analyzer) estimated the total uptake by extrapolating the breakthrough curves to infinite time under the assumption of an exponential approach to saturation. It is important to note that no measurable oxidation occurred during the uptake process in either set of experiments. The SO_2 mixing ratios used by both C and CL ranged between 15 and 100 ppb at normal atmospheric pressure. Hence, with temperatures below −1°C both experiments are clearly in the stability domain of ice (Fig. 1).

The packed beds of ice were prepared by both C and CL in a similar manner. Thus, differences in the morphology of the ice samples are expected to be of minor importance. In each case, droplets of distilled water were allowed to fall into a liquid nitrogen bath, where they froze to form ice spheres of approximately 200 μm in diameter. These spheres were packed into an ice-coated glass tube and then allowed to sinter together at a constant temperature (at −6°C in the CL experiments, and −25°C in C's experiments) over a period of several days prior to an experimental run. The aging process stabilized the ice samples

against significant changes in specific surface area. Thin-section analysis showed that the samples were highly polycrystalline, contained many ice–ice ("grain") boundaries, veins and nodes, and had porosities close to 0.4 (i.e., 40% of the total volume was open to air) (1).

The main differences between the two setups were the lengths L of the packed ice beds ($L = 0.25$ m in CL's and $L = 0.125$ m in C's experiment) and, hence the exposed surface areas. As will be shown later, these differences are responsible to a large degree for the differences between the data sets obtained from the two sets of experiments. Also, C and CL determined the total surface area A_{ice}^{tot} differently. Whereas C used stereology, an optical method, CL measured the flow resistance of the packed ice bed. It is unfortunately difficult to assess the systematic errors introduced by either of these different methods of surface area determination. The specific surface area determined by the flow-resistance method varied between 30–70 m² kg⁻¹, indicating a factor of 2 variability from sample to sample. In our analysis we use the average values $A_{ice}^{tot} = 3.17$ m² for the CL data and $A_{ice}^{tot} = 1.04$ m² for the C data. As we show below, this difference in available surface area contributed substantially to the divergence of findings in the C and CL studies.

2.2. Analytical Approach

The nature of the interaction mechanism determines the form of the breakthrough curve and the accumulated uptake. In order to constrain the likely interaction mechanisms, we compared the observed breakthrough curves with theoretical predictions for different assumed mechanisms. In the Appendix we have therefore derived $p_{out}(t)$ for three candidate mechanisms: (a) diffusive uptake of a nondissociating gas (Eq. [A.6], in the Appendix), (b) diffusive uptake of a dissociating trace gas (Eq. [A.7]), and (c) adsorptive uptake of a nondissociating trace gas (Eq. [A.8]).

The main kinetic model used in this paper is based on Eqs. [A.6] and [A.8], which can be used directly for a nondissociating gas or a dissociating species (only for very short exposure times, Eq. [A.7] must be used). For all but the shortest uptake times we have

$$p_{out}(t) = p(L, t) = p_{in} \exp\left(-\frac{\epsilon A_{ice}^{tot}}{v V_{air}} H^* \sqrt{\frac{D}{\pi t}}\right) \quad [1]$$

and

$$H^* \approx H_0 + \sqrt{\frac{K H_0 k_B T}{p_{in}}}. \quad [2]$$

Here, $V_{air} = F L/v$ is the volume of the packed bed filled by air, F is the volumetric flow rate of air through the column of length L, v is the flow velocity, D (m² s⁻¹) is the diffusion coefficient for SO₂ in the ice reservoir, H^* is the dimensionless Henry's law constant (which takes the possibility of dissociation of the species upon

uptake into account), and ϵA_{ice}^{tot} is the ice surface area effectively available for uptake (ϵ is analogous to the "effectiveness factor" mentioned by Keyser and Leu (24)). Note that $\epsilon = 1$ if the uptake reservoir covers the entire surface, but $\epsilon < 1$ if uptake occurs only at certain locations, such as grain boundaries, veins, or nodes. The effective Henry's law constant, H^* describes the overall solubility of SO₂ in the packed bed, i.e., in all possible reservoirs, such as the ice matrix, grain boundaries, or veins. This parameter also accounts for both the molecular and ionic components of the dissolved trace gas, provided that dissociation occurs. In Eq. [2], H_0 is the dimensionless Henry's law constant describing the solubility of the hydrated but undissociated species, K is the dissociation constant, k_B is the Boltzmann constant, and T is the temperature.

In Eq. [1] there is only one free parameter, $\epsilon H^* D^{1/2}$, which has to be determined from the experiments. In order to determine the fit for $\epsilon H^* D^{1/2}$ from the breakthrough curves, we used the latter part of the signal, where diffusion appears to be the dominant uptake process, excluding the initial, nondiffusive part, where nondiffusive processes are still confusing the picture. That is, we used all the data in an interval (t_{min}, t_{end}) chosen to optimize the fit between the data and calculations from Eq. [1]. The sensitivity of the best-fit parameters to variations in t_{min} gives an estimate of the uncertainties in these fitted values. We calculated $\epsilon H^* D^{1/2}$ for $t_{min} = 1, 3, 5, 7, 10$ h. The choice of t_{min} did not systematically change the value we obtained for $\epsilon H^* D^{1/2}$.

3. RESULTS

3.1. Fractional Coverage

The results from the C and CL experiments may be expressed in terms of a fractional coverage of the ice surface by the SO₂. The effective coverage $\theta(p_{in}, T, t)$, defined as the number of SO₂ molecules taken up by the ice during the time interval $(0, t)$ divided by the number of molecules in a complete monolayer on the ice surface, is related to the upstream and downstream partial pressures (p_{in} and $p_{out}(t)$, respectively) via

$$\theta(p_{in}, T, t) = \frac{F a_0}{A_{ice}^{tot}} \int_0^t \frac{p_{in} - p_{out}(t')}{kT} dt', \quad [3]$$

where $a_0 = 10^{-19}$ m² is the approximate area occupied by a molecule in a surface monolayer.

Figure 2 shows the effective coverage $\theta(p_{in}, T, t_{end})$ as determined by C and CL. The major experimental findings by C and CL, illustrated by the data plotted in Fig. 2, are as follows:

• Large SO₂ coverages were found by CL (about 50 times more than was found by C);
• SO₂ uptake increased with increasing temperature (over the range from −60 to −1°C);
• SO₂ uptake increased less than linearly with increasing mixing ratio (over the range from 15 to 100 ppb).
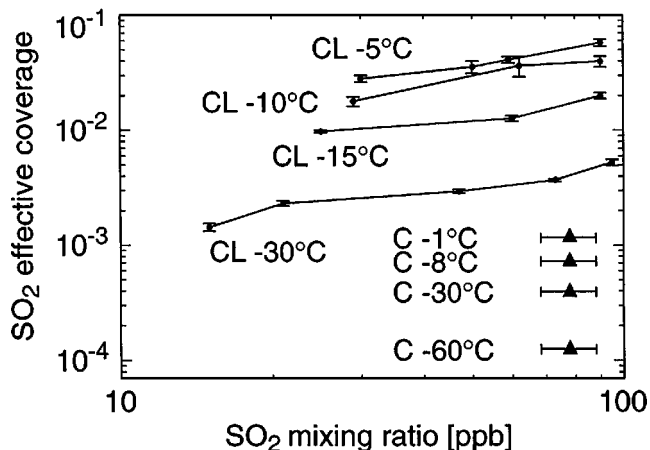
FIG. 2. Effective coverage of SO_2 derived from the measurements by CL (1) and C (2). An effective coverage $\theta = 1$ corresponds to an uptake of 10^{19} molecules of SO_2 per square meter of ice. Error bars indicate the uncertainties of the data as given by the authors. (Figure taken from (63)).

Interpretation of the data in terms of uptake mechanisms must explain these properties of the time-integrated uptake, as well as the kinetics of the process (as represented by the breakthrough curves). The important clues to the uptake mechanism are the remarkable differences in the amounts of SO_2 taken up in the two experiments and the observed anomalous temperature dependence found in both experiments.

3.2. Time Dependence of Uptake

Comparisons of time-resolved data with calculations from various kinetic models serve to identify possible mechanisms of uptake. Figure 3 shows a typical breakthrough curve. The crosses represent data from CL for p_{in} corresponding to 25 ppb at normal pressure (10^5 Pa) and $T = -15°C$, whereas the solid
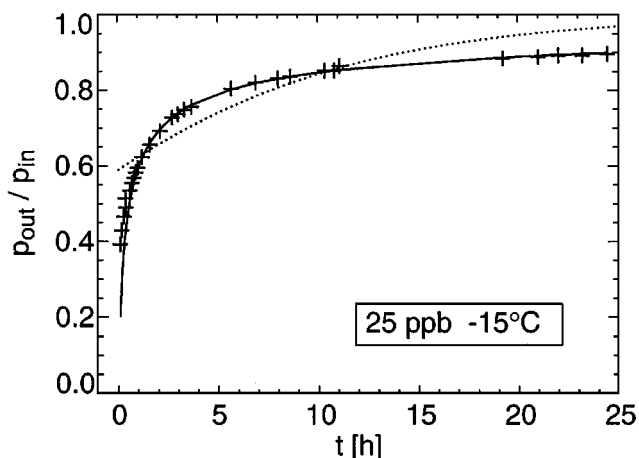

FIG. 3. A typical SO_2 breakthrough curve by CL. Crosses: Breakthrough data as measured by Clapsaddle and Lamb (1) for the case of 25 ppb SO_2, $-15°C$. Solid line: fit to Eq. [1]. Dotted line: fit to Eq. [A.8]. (Figure taken from (63)).

curve shows the best fit to the data assuming purely diffusive uptake (Eq. [1]). The dotted curve in Fig. 3 results when simple adsorption is assumed to occur without dissociation (Eq. [A.8]). Although only one fitting parameter, namely $\epsilon H^* D^{1/2}$, can be used for the diffusive-uptake model, whereas two parameters (k_a and k_d) are adjustable in the adsorption model, the fit is clearly better for diffusive uptake. In both cases we assumed $p_{out}(t \rightarrow \infty) = p_{in}$. We performed a similar analysis on the other 13 experiments performed by CL, those for $-5°C$, $-10°C$, $-15°C$, and $-30°C$ over the experimental range of SO_2 partial pressures, and found equally good agreement with the diffusive uptake model for $t > 1$–3 h. The agreement for the initial period was not particularly good, presumably because other processes, such as wall effects in the gas-flow system and adsorption, likely dominated.

Given some confidence that a model based on diffusion kinetics is appropriate, we next seek common ground between the empirical results of C and CL. The greatest likelihood for success exists when the temperatures and imposed partial pressures of the two experiments are similar, as in Fig. 4, where a logarithmic scale was chosen in order to facilitate the comparison. The data from C (solid dots) were taken at $-1°C$ with p_{in} corresponding to 68–89 ppb at normal pressure (10^5 Pa) (curve in Fig. 2a of C). As shown in Fig. 4a, we applied Eq. [1] to the experimental results from CL (crosses) for p_{in} corresponding to 90 ppb at normal pressure and $T = -5°C$ for their experimental setup: $L = 0.25$ m, $F = 830$ cm^3 min^{-1}, and $A_{ice}^{tot} = 3.17$ m^2. The solid curve is based on the best-fit value of $\epsilon H^* D^{1/2} = 2.7 \times 10^{-4}$ m s$^{-1/2}$. The dotted line is the breakthrough curve calculated for the conditions used by C ($L = 0.125$ m, $F = 600$ cm^3 min^{-1}, $A_{ice}^{tot} = 1.04$ m^2) with the same value for the fitting parameter. Whereas the model does not yield complete agreement with the breakthrough curves of C, some improvement has been achieved by taking account of the different experimental setups within the framework of the kinetic model.

Figure 4b shows the integrated effective coverage θ (90 ppb, $-5°C$, t) calculated from Eq. [3] for the same measurements of CL (as shown by the crosses in Fig. 4a). The horizontal arrow in Fig. 4b shows the equilibrium coverage estimated by CL on the basis of their exponential extrapolation. The diffusive model suggests that uptake should continue well above this limit, provided the diffusion depth ($\sqrt{Dt}$) remains smaller than the radii of the ice grains in the packed bed (i.e., provided that the reservoir does not saturate). The asymptote (straight line in Fig. 4b), as derived from Eqs. [1] and [3], is given by

$$\theta(t \gg t_0) \rightarrow \frac{2a_0 \epsilon H^* p_{in}}{k_B T} \sqrt{\frac{Dt}{\pi}}, \qquad [4]$$

where the threshold time $t_0 = (L A_{ice}^{eff} H^*/(v V_{air}))^2 D/\pi$ ($t_0 \approx 1$ h for the CL and $t_0 \approx 15$ min for the C experiments). If diffusion of SO_2 into a large reservoir is indeed the main uptake mechanism, the effective coverage should be expected to increase, along the asymptote, in proportion to $\sqrt{t}$.
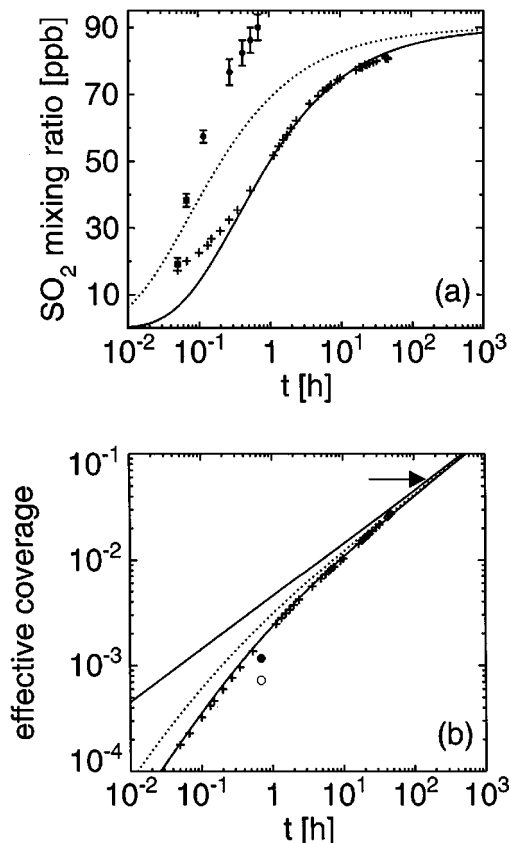
FIG. 4. (a) Breakthrough curves as measured by CL for $-5°C$ and 90 ppb SO₂ (crosses) and by C for $-1°C$ and 69–89 ppb SO₂ (solid dots). Error bars for C are inferred from graphical reading from Fig. 2a in C. Solid line: fit of the data of CL to Eq. [1] yielding $\epsilon H^* D^{1/2} = 2.7 \times 10^{-4}$ m s$^{-1/2}$ with ($A_{ice}^{tot} = 3.17$ m², $F = 830$ cm³ min^{-1}). Dotted line: calculated breakthrough curve using $\epsilon H D^{1/2}$ from CL's data and the experimental conditions of C's experiment. ($A_{ice}^{tot} = 1.04$ m², corresponding to a tube length of 0.125 m, $F = 600$ cm³ min^{-1}.) (b) Effective coverage corresponding to the two cases in (a). Crosses and solid curve: integrated results for CL calculated from Eq. [3]. Dotted curve: calculated coverage in C's experiment using $\epsilon H D^{1/2}$ as derived from CL's experiment. Dots: coverage as determined by C via liquid-phase analysis. (Solid dot, $-1°C$; open dot, $-8°C$.) The straight line is the asymptote according Eq. [4]. The horizontal arrow shows the coverage determined from CL's exponential extrapolation. (Figure taken from (63)).

The dots in Fig. 4b show the corresponding effective coverage from the C experiments based on their liquid-phase analysis of the melted ice at the conclusion of the experiment for $-8°C$ (open dot) and $-1°C$ (solid dot). The largest part of the apparent discrepancy (more than a factor of 70) between this value (approximately 8×10^{-4}) and that (horizontal arrow, 6×10^{-2}) obtained by CL is due to the different tube lengths (and to a smaller extent different volumetric flow rates)—i.e., to different values of t_0 for the two experiments and the exponential extrapolation used by CL (horizontal arrow in Fig. 4b). In effect, the exposure time required to reach apparent saturation of the column in the CL experiment is 4 times longer than that in the C experiment. The remaining discrepancy of less than a factor of 3 between the two data sets (open dot in Fig. 4b vs cross at the

same time) may be caused by experimental uncertainties, surface uptake, different ice packing densities, or slightly different sintering parameters. As noticed by C, their value (open dot) is not entirely consistent with their breakthrough curve (solid dots in Fig. 4a). Such a discrepancy might arise from a drift in the SO₂ gas analyzer, as mentioned by C, and could partially explain the relatively poor comparison of their data with the diffusive model. In addition, nondiffusive processes might be more important during the shorter duration of C's experiments compared to those of CL. We note also that CL's breakthrough curves deviate from the diffusive kinetics during the first 1–3 h as discussed above (cf. Fig. 4b).

4. DISCUSSION

The results of this study offer new insights into the behavior of SO₂ in contact with polycrystalline ice. The kinetic model is able to explain the time dependence of the CL laboratory data very well, at least beyond the first 1–3 h of contact. Moreover, the integrated amounts of uptake measured by the two separate laboratories (C and CL) are seen to be consistent with each other within the context of our diffusive uptake model. The kinetics of the observed uptake suggest a slow diffusive process, although the uptake reservoir has yet to be established. As a way of constraining the possible uptake mechanisms further, we have compared the major features of the observed uptake with those predictable from a set of conceivable processes. The compatibility of each process with the available data is presented in Table 1, parts of which are detailed in this section. The main observations to be explained are the pressure and temperature dependencies of the uptake, the observed kinetics, and the rather large size of the implied reservoir.

4.1. Bulk Reservoirs: Liquid Water, Ice Matrix

The magnitude of the fitting parameter ($\epsilon H^* D^{1/2}$) used in the kinetic model reveals information about the asymptotic behavior of uptake (via Eq. [4]), as well as about the nature of the gas–ice interaction in general. To see how important the ice lattice itself might be in taking up SO₂, we estimated the apparent ice–water partition coefficient for SO₂ (defined as the ratio of overall solubilities in ice and liquid, $K_{sl} \equiv H_{sc}^*/H_{liq}^*$). The apparent Henry's law constant in a single crystal (H_{sc}^*) was estimated from the diffusivity of trace gases in single crystals D_{sc} and the packed-bed results under the assumption that $\epsilon = 1$: for $-5°C$, we find $H_{sc}^* = (H^* D^{1/2})_{exp}/D_{sc}^{1/2} \simeq 3 \times 10^4$. This value is approximately equal to H_{liq}^*, yielding an inferred partition coefficient of $K_{sl} = H_{sc}^*/H_{liq}^* \simeq 1$, which would imply equal solubilities of the trace gas in water and the ice crystal. By contrast, measured values of the partition coefficient for ionic species are typically well below 10^{-2} (44). Thus, the large observed uptake of SO₂ cannot be accounted for by diffusion into the crystal lattice.

The amount of SO₂ taken up in the packed-bed experiments is large, as is most easily seen by calculating the fraction of

TABLE 1
Comparison of Different Uptake Processes and Their Compatibility with the C and CL Ice Packed Bed Experiments[a]

	Magnitude of uptake	Pressure dependence	Temperature dependence	Kinetics
Ice lattice	$(-)$ Observed uptake too large	$(\pm)$ Expect $\sim p^{1/2}$, but if defects are involved then expect $\sim p^{1/3}$	$(-)$ $T \downarrow \Leftrightarrow \theta \uparrow$, contrary to observation	$(+)$ $D_{sc} < 10^{-16}\ m^2\ s^{-1}$
Bulk water	$(-)$ Observed uptake too large	$(+)$ $\sim p^{1/2}$, Expect dissociation	$(-)$ $T \downarrow \leftrightarrow \theta \uparrow$, contrary to observation	$(-)$ $D_{liq} > D_{max}$, but observed kinetics shows no saturation
Adsorption	$(+)$ $\theta \sim 10^{-3}$–10^{-4} are acceptable values	$(\pm)$ Unknown	$(-)$ $T \downarrow \leftrightarrow \theta \uparrow$, contrary to observation	$(-)$ Breakthrough curve contrary to observation; see Fig. 3
Veins	$(\pm)$ Wall effects may enhance uptake	$(+)$ $\sim p^{1/2}$, Expect dissociation	$(+)$ $\sim (T - T_0)^{-1.1}$, $H^* D^{1/2}(T)$; see text	$(+)$ Proximity of walls may decrease diffusivity
Grain boundaries	$(\pm)$ Wall effects may enhance uptake	$(\pm)$ Expect dissociation; wall effects may be important	$(\pm)$ Unknown	$(+)$ Proximity of walls may decrease diffusivity
QLL	$(-)$ Observed uptake too large (see Table 2); interface may enhance H^*_{QLL}	$(\pm)$ Expect dissociation; wall effects may be important	$(-)$ $\sim (T - T_0)^{-1/3}$; temperature dependence weaker than observed	$(-)$ QLL expected to saturate quickly

[a] $(+)$ indicates the data are compatible with the model predictions for this reservoir. $(-)$ indicates the data are incompatible with the model predictions for this reservoir. $(\pm)$ indicates compatibility cannot be determined. For description see text. Diffusivity in single crystals D_{sc}, in the liquid phase D_{liq}, maximum diffusivity without saturation within the experimental time scales of the CL experiment D_{max}. "Wall effects" refers to the possibility of enhanced integration of solute molecules into the transition region between the crystalline ice matrix and the liquid phase in veins, grain boundaries, or QLL, due to the specific nature of matter in these small reservoirs.

water in the ice sample that would be in a liquid state were the uptake reservoir to be bulk water in equilibrium with the given gas-phase partial pressure. This fraction is shown in the third column of Table 2, where the effective Henry's law constants for SO$_2$ in supercooled water have been estimated for the indicated temperatures (37). The last column of Table 2 expresses this liquid fraction as an equivalent thickness of a liquid shell that would coat the surface of ice spheres 100 μm in radius. In the experimental case at $-5°$C and 90 ppb SO$_2$, for instance, more than half of the sample would have been liquid, forming a wet mush. Such a sample state was not observed, and it would moreover be inconsistent with the ice–SO$_2$ phase diagram (Fig. 1). The partial pressures of SO$_2$ used by C and CL were far too small to cause the ice to melt. The calculated fractions and depths of liquid, especially at the higher temperatures, are physically unreasonable and suggest that a reservoir other than bulk liquid was active.

The empirical dependence of $\epsilon H^* D^{1/2}$ on p_{in} does, nevertheless, reveal behavior similar to that of trace gas interactions with liquid water. (Any dependence of the effective Henry's law constant (H^*) on solute concentrations and hence on the trace gas pressure will be reflected directly through $\epsilon H^* D^{1/2}$, since $D^{1/2}$ is not expected to depend on concentration or pressure.) Figure 5 shows the variation of the $\epsilon H^* D^{1/2}$ values derived from the CL ice-bed experiments with the applied SO$_2$ partial pressure. (The

error bars show the variation in the fitted $\epsilon H^* D^{1/2}$ values due to the choice of different fitting intervals from the different CL data sets.) The solid lines are fits to the data at $-30°$C and $-15°$C, yielding pressure dependencies of $\epsilon H^* D^{1/2} \propto p_{in}^{-0.45}$ and $\epsilon H^* D^{1/2} \propto p_{in}^{-0.48}$, respectively. As shown in the Appendix, and by Eq. [2], a species that dissociates upon dissolving in water exhibits a pressure dependence $H^* \sim p^{-1/2}$. Even though the calculated exponents for higher temperature CL data show much greater scatter, they too suggest that SO$_2$ very likely dissociates during the uptake into polycrystalline ice. This conclusion, based on an analysis of the uptake kinetics, corroborates the interpretation given by CL (based on their total uptake analysis). A $p_{in}^{1/2}$ dependence of θ was also found by other authors (39, 41), giving further indication for the involvement of a liquid or liquid-like reservoir in the uptake process.

The temperature dependence of the measured SO$_2$ uptake in the ice beds is quite distinctive and provides an important clue for identifying the uptake process. In Fig. 6 we show the value of $\epsilon H^* D^{1/2}$ as derived from the CL data normalized to the value at $-5°$C as a function of inverse temperature. The data have been divided into three ranges in order to account for the pressure dependence of the uptake: range I, 1–23 ppb; range II, 47–73 ppb; range III, 90 ppb. The solid line in Fig. 6 shows the temperature dependence of the Henry's law coefficient of SO$_2$ in bulk water, as calculated from the Henry's law coefficient of

TABLE 2

Amount of Melt Water in the Ice (if SO₂ Reservoir Is Liquid Water) That Was Necessary To Account for the CL Experimentally Measured Uptake[a]

$T - T_0$ (°C)	p_{SO_2} (ppb)	Liquid fraction	Equivalent layer thickness (μm)
−5	59	0.42	17
	90	0.53	22
−10	29	0.23	8.4
	62	0.32	12
	90	0.29	11
−15	25	0.11	3.8
	60	0.10	3.3
	90	0.11	3.7
−30	15	0.012	0.51
	21	0.015	0.51
	47	0.013	0.44
	73	0.013	0.45
	93	0.018	0.60

[a] Third column: amount of melted water expressed as fraction of total water in the packed bed. Fourth column: amount of melted water expressed as liquid layer thickness on surface of 100 μm ice sphere. These unphysically large liquid fractions suggest that the SO₂ reservoir is not bulk liquid water or a quasi-liquid layer.

SO₂ in water. Whereas the uptake of a gas by bulk liquid water normally decreases with increasing temperature because of reduced solubility at higher temperatures, the packed-bed experiments are very consistent in showing the opposite behavior. Even after accounting for a reasonable temperature dependence for the diffusion coefficient, we still find inadequate agreement with the data (see dashed curve in Fig. 6).

For the ice lattice, the temperature dependence of the quantity $\epsilon H^* D^{1/2}$ can only be estimated, as there are neither solubility nor diffusivity data for SO₂ interacting with single ice crystals. But a comparison with similar systems, such as HNO₃ uptake into single ice crystals by Thibert and Dominé (16) or uptake of
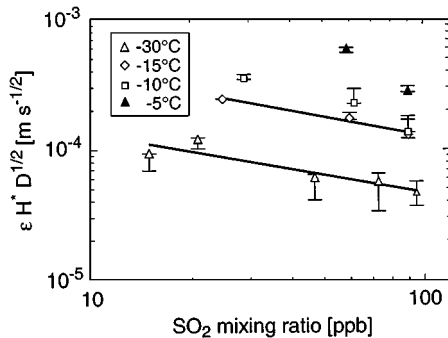
FIG. 5. Best-fit values for $\epsilon H^* D^{1/2}$ determined from Eq. [1] for the measurements of Clapsaddle and Lamb (1) as a function of SO₂ mixing ratio. The solid lines are fits to the data subsets at −30°C and −15°C showing $\epsilon H^* D^{1/2} \propto p^{-1/2}$. (See text for explanation of error bars. Figure taken from (63)).
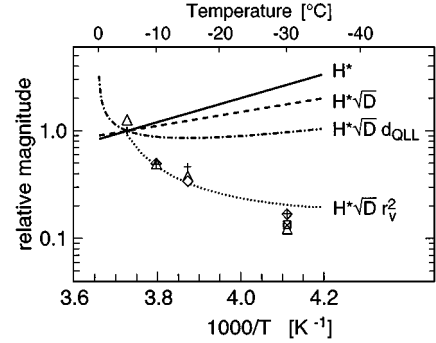
FIG. 6. Dependence on temperature T of the packed ice bed results compared with various quantities, normalized to the value at −5°C. Solid line: solubility of SO₂ in water. Dashed line: $H^* D^{1/2}$ for SO₂ in water. Dash-dotted line: $H^* D^{1/2} d_{QLL}$ for uptake into a quasi-liquid layer (QLL), assuming $d_{QLL} \propto (T - T_0)^{-1/3}$. Dotted line: $H^* D^{1/2} r_v^2$ for uptake into veins. CL-data: squares, 15 ppb; diamonds, 21–29 ppb; star, 47 ppb; triangles, 50–73 ppb; crosses, 90 ppb. To account for the pressure dependence of uptake, the CL data have been divided into bins (15 ppb, 1–29 ppb/47–73 ppb/90 ppb). These bins have been normalized internally at −10°C, since only two data sets are available at −5°C. (Figure taken from (63)).

HNO₃ into supercooled water, shows them to exhibit a normal temperature correlation, similar to that shown by the dashed curve in Fig. 6 and in clear conflict with the ice bed data. Simple diffusion of SO₂ into either bulk water or bulk ice is therefore not viable as the uptake mechanism.

4.2. External Interfacial Reservoirs: QLL and Surface Layer

If the uptake reservoir were a surface-melted layer (or QLL) at the air–ice interface, then the volume of the uptake reservoir might well increase with increasing temperature and offer an explanation for the observed temperature dependence of uptake. Experiments attempting to measure the thickness increase as the temperature T approaches the ice melting temperature T_0 show widely varying results, with reported QLL thicknesses at −2°C ranging from less than 0.1 to 80 nm (26, 28, 30–32, 45–47). Nevertheless, any increase in layer thickness with an increase in temperature would serve to counter the normal tendency of gas solubility to be lower at higher temperatures. Indeed, such an argument has been used to explain data by a number of other authors (e.g., (17, 34)). From a theoretical point of view (see (3) for a review), we note that if the thickness of the layer, $d_{QLL}(T)$, were independent of the chemical composition or other electrostatic effects (48) and if van der Waals forces were to dominate the overall behavior of the layer, we would expect a temperature dependence $d_{QLL} \propto (T - T_0)^{-1/3}$. We thus obtain a normalized uptake ($H^* D^{1/2} d_{QLL}$) as given by the dash-dotted curve in Fig. 6, a trend with temperature that is too weak at low temperatures and too strong at high temperatures for agreement with the data.

We furthermore emphasize that neither the holding capacity of any realistic QLL nor the kinetics of uptake into such an interfacial layer are able to explain the experimental data. We have

already seen that the amounts of SO_2 taken up by the packed beds would require unrealistically thick layers, short of invoking some unknown surface interaction. Transport of the solute throughout the QLL by diffusion, too, gives untenable results. For instance, measurements of the self-diffusion coefficient for the QLL (29) yield the relationship $D_{liq} \gg D_{QLL} \approx 10^{-13}$ m^2 s$^{-1} > D_{max} \approx 3 \times 10^{-14}$ m^2 s^{-1}, where D_{liq} is the liquid-phase diffusivity. From the time scale of CL's experiments (up to 48 h) and the size of the ice spheres (100 μm radius) saturation effects must occur for diffusivities higher than D_{max}. Even though diffusion within a QLL is much slower than diffusion in a liquid, the reservoir would easily saturate within the time frame of a typical experimental run. The QLL is not likely to be the uptake reservoir sought for consistency with the SO_2 packed-bed findings.

4.3. Internal Interfacial Reservoirs: Veins, Nodes, and Grain Boundaries

Of all the reservoirs into which SO_2 can be stored following uptake, only the class of ice–ice boundaries remains viable. Unlike the air–ice interface, the grain boundaries, veins, and nodes so characteristic of polycrystalline ice offer significant volumes and surface areas within a polycrystalline bed for harboring small molecular species like SO_2 and its dissociation products (e.g., HSO_3^-). Past studies have shown the importance of grain boundaries and especially veins for accumulating species like H_2SO_4 and HCl (12, 49) as well as the existence of ions in the veins (50) and therefore the liquid-like character of veins. Thus it is reasonable to consider ice–ice boundaries as solute reservoirs in the SO_2–ice system as well.

Grain boundaries are conceivably important because of the large interfacial area (and consequently new volume) potentially available to solute within the ice matrix itself. If the temperature dependence of the grain boundary width is similar to that for the thickness of the QLL and if the local roughness of the grain boundary walls is unimportant in determining the interfacial melting (51), then the same fundamental parameter ($H^*D^{1/2}d_{QLL}$) used to estimate the action of the QLL also reflects the temperature dependence of a diffusion process into grain boundaries. We are again left with the dash-dotted line in Fig. 6 and see that grain boundaries, too, give a temperature trend that is inconsistent with that of the observations.

Veins and nodes, however, offer a significantly different opportunity for solute storage. For one thing, the network of veins inside a polycrystalline sample can be extensive: an order-of-magnitude calculation suggests lengths ~30 m cm^{-3} (based on a cubic grain size of 100 μm). A proper determination of the total reservoir volume due to veins and nodes in the packed beds used by C and CL would have required a microscopic investigation of the ice samples, a procedure not performed at that time. Nevertheless, we would not expect such a reservoir to saturate readily, especially because viscosity effects associated with the close proximity of the ice walls would tend to decrease the dif-

fusivities of impurities in these reservoirs relative to those in bulk liquid water. The diffusivity in veins and grain boundaries is unknown, but it is likely to be intermediate between that in ice and that in supercooled water (29, 52).

The vein cross sections, and hence reservoir volumes in polycrystalline ice, should be particularly responsive to temperature changes. Although we have shown that the bulk melting point is not depressed significantly at the SO_2 partial pressures used in the C and CL experiments, interfacial effects within the veins can depress the melting point substantially. In particular, Colbeck (20) has found that the melting point is locally depressed as a result of the curvature of the grains along the veins and necks between adjacent ice grains, an interfacial phenomenon that does not show up in traditional bulk-phase diagrams (e.g., Fig. 1). The magnitude of the melting point depression in veins and nodes has been treated theoretically by Nye (21), who extended the work of Colbeck (20) by considering solute effects as well. The objective of the Nye studies, as well as those of experiments performed by Mader (22, 23), was to examine heat and solute flow during warming and cooling of polycrystalline ice. The theoretical dependence of the radius of curvature of ice in contact with vein fluid on the deviation of the temperature away from the melting point T_0 was found to be $r_v(T) \propto (T_0 - T)^{-0.55}$ (21), a result corroborated by Mader's observations (22, 23). The equilibrium concentration of an impurity in the veins and the vein radii are determined by the temperature and the interfacial energies of the liquid/solid boundaries (21). These impurities are all nonvolatile species expelled from the ice matrix during the freezing process into the veins and grain boundaries (typically sulfates and salts) and in addition the dissolved gaseous SO_2. We cannot treat the influence of the nonvolatile impurities explicitly here, because amount and species are unknown for both experiments.

The observed temperature trend of SO_2 uptake is consistent with Nye's theory of solute in veins and nodes. Under the assumption that the solute solubility and diffusivity in a vein have the same temperature dependencies as in bulk liquid water, the predicted uptake varies as $\epsilon H^*D^{1/2}$, with $\epsilon = A_{ice}^{eff}/A_{ice}^{tot} \propto r_v^2 \propto (T_0 - T)^{-1.1}$. The resulting temperature dependence is shown as the dotted curve in Fig. 6, revealing relatively good agreement with the data obtained by CL. In effect, the expansion of the vein cross section with increasing temperature opens up new opportunities for SO_2 to enter the ice sample, resulting in larger reservoir volumes and transport channels and thus greater apparent magnitudes of uptake. The temperature dependence of this volume effect more than compensates for the decrease in gas solubility (H^*) at higher temperature (reflected in the solid curve in Fig. 6). The nodes in the ice bed exhibit their own temperature dependence, which is proportional to $r_v^3 \propto (T_0 - T)^{-1.65}$, introducing an effect that would lower the dotted curve somewhat and lead to still better agreement with the observations.

It is important to note, however, that the case at hand differs from these other studies in the following ways: (a) the ice grains and the veins in the experiments of Mader and considered in

the theory of Nye were substantially larger than those in the packed-bed experiments of C and CL and (b) the temperatures examined in the Mader experiments were at most a few tenths of a degree below the triple point. Over such a small temperature range, curvature effects on the depression of the melting point tend to be smaller than solute effects. However, this is not the case for the temperatures of the packed-bed experiments, where the temperature effect should theoretically dominate.

Of the diverse options considered, the uptake kinetics of SO_2 into polycrystalline ice seem most likely to be governed by veins and nodes. Whereas the veins and nodes themselves may be the main reservoir for the trace gas uptake, we must acknowledge the possibility that the veins also serve as the transport channels of the dissolved gas into some larger reservoirs. We note, too, that prior to attainment of equilibrium, the rate-limiting process determines the nature of the uptake kinetics and masks possible equilibrium properties, such as those arising from adsorption or electrical effects at the vein solution–ice interface. For many experimental and environmental applications, diffusion of SO_2 or its dissociation products through the veins appears to determine the overall kinetics of uptake.

4.4. Applications to Ice in the Environment

Uptake of SO_2 by ice in the environment modifies the atmospheric chemical composition, as well as the chemical character of precipitation, snowpacks, and glacier ice. Acidic precipitation, for instance, has long been a major topic of environmental research, with anthropogenic sulfur dioxide and nitrogen oxides identified as the main gaseous precursors of liquid-phase acids (see Lelieveld (36) for an overview). In addition, the sulfate concentrations in ice cores reveal information about the atmospheric sulfur load in the distant past (53). Diffusion of the solutes in grain boundaries and veins might have important consequences for the interpretation of the ice core results. Therefore, it is of particular interest to understand the mechanism of uptake of sulfur dioxide by environmental ice.

The concentrations of grain boundaries, veins, and nodes within atmospheric ice have not been characterized in detail, and they are expected to depend on the mechanism of ice formation (54). Comparisons of uptake measurements of SO_2 by atmospheric ice and by laboratory ice samples are problematic because the percentages of ice–ice boundaries in the two regimes may differ considerably. As yet, there exists no recipe for making "atmospheric ice" in the laboratory. Still, laboratory experiments, in which the ice preparation is carefully controlled and the history of uptake can be followed in time, are useful for deciphering mechanisms and for empirically relating the concentration of a precursor in the gas phase to that in the ice.

Since diffusive processes may govern the long-term uptake of trace gases by environmental ice and considerably enhance the short-term uptake, care must be taken both when making measurements and when applying atmospheric models. The total uptake can be used directly only if the experimental time scales are long enough to observe reservoir saturation and the diffusive kinetics are parameterized in an appropriate manner. If, as the present analysis implies, veins and nodes govern the uptake of trace gases, then the ice morphology (i.e., the ice grain size and vein density) must be considered. Otherwise, the results of the uptake experiments on laboratory ice may not be directly applicable to natural ice.

In the atmosphere, uptake of SO_2 on cloud ice is likely to be accompanied by oxidation, so the CL experiments (and our analysis of them) do not represent the full range of processes operative in nature. On intermediate time scales, the uptake on freshly fallen snow may well be similar in several respects to the laboratory observations, in which case the observed pressure and the temperature dependence of the uptake developed here could be translated into parameterizations for atmospheric models. More generally, however, the absolute magnitude of the uptake of sulfur species found in the laboratory will be less than would be found in the atmosphere due to oxidative processes.

An interesting parallel can be drawn between our interpretation of the laboratory results and the dry deposition of a trace gas to surface ice. In order to resolve the different components of the overall uptake process, a surface resistance concept may be used as in conventional dry deposition schemes. Following the definitions of Voldner et al. (55), one calculates the deposition velocity v_d (with, $v_d = j_{net}c^{-1}$, where j_{net} is flux and c is the ambient concentration of gas) as the inverse of the overall resistance $r_t = 1/v_d$, which in turn is the sum of the resistances of the individual uptake processes: $r_t = r_a + r_b + r_s$, where r_a is the aerodynamic resistance due to turbulent transfer in the air, r_b is the resistance due to molecular diffusion across the laminar sublayer, and r_s is the resistance due to pollutant–surface interactions.

Our interpretation of the packed-bed experiments suggests that in the absence of oxidative processes the surface resistance of SO_2 on fresh snow should follow the proportionality relation

$$\frac{1}{r_s} = \epsilon(T) \times \frac{H^*\sqrt{D}}{\sqrt{\pi t}} \propto \frac{1}{(T_0 - T)^{1.1}} \times \frac{1}{\sqrt{pt}}, \quad [5]$$

with p the gas partial pressure, T_0 the melting point of ice, and $\epsilon(T)H^*\sqrt{D}$ derived from the experimental data. This approach considers only the gas–ice interaction, as it ignores the resistance due to gaseous diffusion within the snow pack. Bales et al. (56), on the other hand, considered the gas-phase diffusion into the snow pack as the limiting transport process and assumed an instantaneous equilibrium at the ice surface. The physical conditions of a given snow pack may well determine whether gas-phase or condensed-phase diffusion limits the uptake, but it is interesting that the time-dependent uptake law derived by Bales et al. (56) has the same form as Eq. [5]. Hence, the effective surface resistance in the absence of chemical reactions

is

$$r_s = \left(\frac{1}{\epsilon(T)H^*\sqrt{D}} + \frac{1}{H^*\sqrt{D_g}} \right) \sqrt{\pi t}, \qquad [6]$$

where D_g is the gas-phase diffusivity through the air in the snow-pack. This time-dependent formulation might find use in modeling studies on a local scale for estimating the SO_2 deposition onto fresh snow, at least when oxidative processes can be neglected. Ganzeveld *et al.* (57) used an exponential function to parameterize the temperature dependence of the dry deposition of SO_2, but noted that their model yields too much SO_2 in the northern hemisphere during winter, which might be due to an underestimation of the dry deposition of SO_2 onto snow and ice surfaces. We suggest that parameterizations for the SO_2 uptake in local and global-scale models should reflect the partial pressure and temperature dependence given by Eq. [5]. Use of this new temperature dependence would lessen the fall-off of uptake at lower temperatures and might lead to an improved calculation of SO_2 dry deposition rates.

5. SUMMARY AND CONCLUSIONS

This analysis of the C and CL studies (as summarized in Table 1) suggests that the likely mechanism for the uptake of SO_2 into polycrystalline ice is slow diffusion into an internal reservoir, such as veins and nodes, possibly also within grain boundaries. To a significant extent, the apparent discrepancies between the measured uptakes in the C and CL studies are now resolved. The remaining differences may be due to the different experimental procedures used in the two studies, such as different SO_2 detection techniques, different methods of surface area determination, or different ice-packing and sintering procedures that might affect the specific surface area and morphology of the samples. Although the precise magnitude of uptake must depend on the detailed polycrystalline character of the ice, as determined by the ice preparation, the general form of the breakthrough curves and the temperature dependence of the uptake are expected to be relatively insensitive to differences in experimental procedures.

Because uptake into major reservoirs (i.e., bulk liquid, bulk ice, and the ice-vapor interface) appears unlikely, the large magnitude of the observed uptake implies that the concentration of SO_2 in the confined reservoirs may exceed the gas–liquid equilibrium value. We propose the following possible mechanism for enhancing the gas solubility in veins and grain boundaries. Whereas the negative solute ions (HSO_3^-) are probably confined to the veins for steric, electrical, or energetic reasons, the positive hydronium ions resulting from SO_2 dissociation are relatively free to diffuse throughout the ice sample (58). If f_s represents the fraction of the total sample volume accessible to solute, then charge conservation requires $(1 - f_s)[H^+]_{lattice} + f_s[H^+]_{veins} = [HSO_3^-]$, $[H^+]_{veins} = f_s[HSO_3^-]$. Here $[HSO_3^-]$ is the total ion concentration in the solute, and $[H^+]_{veins}$ and

$[H^+]_{lattice}$ are the proton concentrations in the veins and the ice lattice respectively. The protons in the ice will be concentrated in regions around the veins, of thickness given by the appropriate Debye length. Therefore $[H^+]_{veins}$ will be less than $[HSO3^-]_{veins}$. We thus expect the effective Henry's law constant to be enhanced, possibly substantially, by the factor $f_s^{-1/2}$: $H^* \approx (KH_0k_BT/f_sp)^{1/2}$, where K is the equilibrium constant of dissociation and H_0 the molecular Henry's law coefficient. In effect, the ice matrix acts as a strong sink for protons due to their relatively high mobility in ice. This loss of protons from the vein fluid increases the local pH and shifts the equilibrium in favor of dissolved SO_2. The asymmetric distribution of ions in the ice operates in the correct sense needed to explain the large magnitudes of SO_2 taken up by polycrystalline ice, but a quantitative assessment of the effect is beyond the scope of this work and remains the subject for a future study.

No sulfate was found in the ice by CL after the experiment, excluding oxidation to influence the uptake in their experiments. However, we must acknowledge the possibility that nonvolatile impurities, which may accumulate in the veins and grain boundaries during the freezing of the ice, might alter and possibly enhance the SO_2 solubility in the veins above the solubility in pure water. Such processes cannot be quantified lacking knowledge about species and magnitude of such nonvolatile substances.

We have presented a framework for the systematic analysis of the uptake of a trace gas from laboratory data involving polycrystalline ice. The interpretation of existing data leads to the hypothesis that solute transport through the veins is the rate-limiting step and that the fluid in confined reservoirs (grain boundaries, veins, and/or nodes) constitutes an important uptake reservoir for SO_2. This finding is consistent with the work of Mulvaney *et al.* (49) and Wolff and Mulvaney (12), who suggested that the accumulation sites for H_2SO_4 and HCl are at the ice triple junctions. Similarly, incorporation of both HCl and HNO_3 at defect sites and the impurity transport along one dimensional defects has been proposed by Thibert and Dominé (16, 35). We suggest laboratory tests of such hypotheses may be made by measuring uptake into ice of varying degrees of polycrystallinity and analyzing the liquid in the interstices of the ice following uptake. In general, interpretation of laboratory studies on uptake would be aided by independent studies relating the morphology of ice samples to the preparation method, focusing on the grain boundary/vein/node system.

APPENDIX: THE FLOW TUBE EQUATIONS

We assume the flow to be isothermal and characterized by rapid lateral diffusion, so the trace gas (SO_2) partial pressure $p(x, t)$ depends on a single spatial coordinate (x, the distance downstream from the tube inlet) and on time t. Then, if we ignore diffusion along the flow (x) direction, the mass continuity relationship is

$$\frac{\partial p}{\partial t} + v\frac{\partial p}{\partial x} = P(x, t) - L(x, t), \qquad [A.1]$$

where P and L are the production and loss terms, respectively, and v is the mean velocity of the air through the tube. The SO$_2$ partial pressure satisfies the upstream boundary condition, $p(0, t) = p_{in}$ for all $t > 0$, and the initial condition, $p(x, 0) = 0$ for all $x > 0$.

The production and loss terms can be combined and written in terms of the net flux of molecules toward the ice surface, $j(x, t)(m^{-2} s^{-1})$,

$$P(x, t) - L(x, t) = -j(x, t)A_{ice}^{eff}\frac{k_B T}{V_{air}}, \qquad [A.2]$$

where k_B is the Boltzmann constant, $V_{air} = FL/v$ is the void volume (i.e., that portion of the packed bed filled by air), and A_{ice}^{eff} is the ice surface area that is effectively available for uptake. The effective area (A_{ice}^{eff}) is equal to the total ice surface area A_{ice}^{eff} only if the uptake reservoir covers the entire surface, but more typically $\epsilon = A_{ice}^{eff}/A_{ice}^{tot} < 1$ because uptake tends to be active only at certain locations, such as grain boundaries, veins, and nodes. We assume the net production may also be written in the form

$$P(x, t) - L(x, t) = -p(x, t)/\tau(t), \qquad [A.3]$$

where $\tau(t)^{-1}$ represents the first-order rate coefficient for loss by an as-yet unspecified process. The function $\tau(t)$ is independent of x and p and represents the properties of the empirical system we seek to infer from the data. We show below that the uptake processes of interest here can be cast into this form under certain conditions.

Solution of Eq. [A.1] with Eq. [A.3] used for the net production can be achieved readily with the help of a simple transformation of coordinates from (x, t) to $(x - vt, t)$. The solution is therefore

$$p(x, t) = p_{in}\Theta(t - x/v)\exp\left(-\int_{t-x/v}^{t}\frac{dt'}{\tau(t')}\right), \qquad [A.4]$$

where $\Theta(\xi) = 0$ for $\xi < 0$ and $\Theta(\xi) = 1$ for $\xi \geq 0$. The nominal transit time of gas molecules in the packed ice bed, x/v, is of the order of seconds, while the uptake extends over hours. Hence, $t \gg x/v$ over most of an experimental run, meaning that $\tau(t)$ is approximately constant over the period of integration in Eq. [A.4]. We thus have

$$p(x, t) \approx p_{in}\exp\left(-\frac{x}{v\tau(t)}\right). \qquad [A.5]$$

Note that the time scale $\tau(t)$ measures the exponential time response of the sink at any point along the packed ice bed, at least when the local SO$_2$ partial pressure is relatively fixed in value. To find the characteristic time for the net sink, $\tau(t)$, we assume the surface of the sink to be in instantaneous equilibrium with the local value of $p(x, t)$. That is, the temporal change of the partial pressure at a fixed location x and time t is taken to be small compared to the net loss into the condensed-phase:

$p/\tau(t) \gg |\partial p/\partial t|$. The validity of this approximation must be reconsidered once the sink rate is determined.

The observed uptake of a trace gas by an ice sample is the composite result of several processes operating simultaneously. Here, we consider mainly adsorption onto the surface and diffusive transport into grains, grain boundaries, veins, and nodes. Therefore, we expect the breakthrough curve to have at least two regimes: an initial segment, governed primarily by surface processes, and a second segment dominated by the slower diffusive processes. Together, the surface and bulk transport processes determine the shape of the breakthrough curve $p_{out}(t) = p(L, t)$. In the following, we compute the uptake flux j and the characteristic time τ as functions of time and solve the resulting flow tube equation for each uptake mechanism in order to assess the relative importance of adsorptive uptake and diffusive uptake in the packed-bed experiments.

A.1. Diffusion Kinetics

If the ice sample does not become saturated during the experiments, the ice grains in the packed bed can be approximated by semi-infinite reservoirs with planar surfaces. In this case we solve the one-dimensional diffusion equation $\partial n/\partial t = D\partial^2 n/\partial z^2$, where n is the concentration of SO$_2$ molecules (or associated ions) in the bulk sample, z is the coordinate perpendicular to the ice surface (i.e., depth into the sample), and D is the bulk diffusion coefficient. This equation is solved subject to the boundary and initial conditions $n(x, z = 0, t) = H^*p(x, t)/(k_B T)$, and $n(x, z, 0) = 0$ for all $x, z > 0$. Here, H^* is the dimensionless form of the effective Henry's law constant, a measure of the overall solubility of SO$_2$ in ice (and/or in its grain boundaries/veins). The magnitude of H^* and its dependence on partial pressure depend on whether or not the trace gas dissociates into ions in the ice sample.

Nondissociating species. For a nondissociating species, H^* is a function of temperature but not of the gas partial pressure. From the net diffusive flux density of molecules to the surface, $j = -D\partial n/\partial z = (H^*p/k_B T)(D/\pi t)^{1/2}$ (59, 60), we derive the characteristic time $\tau(t)$ from Eq. [A.2]: $\tau(t) = V_{air}/(A_{ice}^{eff}H^*)(\pi t/D)^{1/2}$. This result satisfies the condition that $\tau(t)$ is independent of x and p and is thus consistent with Eq. [A.3].

We thus obtain, from Eq. [A.5], the time-dependent partial pressure at the exit of the flow tube

$$p_{out}(t) = p(L, t) = p_{in}\exp\left(-(t_0/t)^{1/2}\right), \qquad [A.6]$$

where $t_0 \equiv (LA_{ice}^{eff}H^*/(vV_{air}))^2 D/\pi$. The parameter t_0 is a measure of the time response of the exit pressure in the gas that has passed over the entire ice bed. A similar equation, with $\epsilon = 1$, was used by Hanson and Ravishankara (61) for interpreting trace-gas uptake on liquids.

Dissociating species. If SO$_2$ dissociates during uptake, the Henry's law constant becomes pressure dependent and the uptake kinetics change. For instance, the dissolution of SO$_2$ into

acidic water (i.e., when the second dissociation can be ignored) is described by the following equilibria: $SO_2(g) \rightleftharpoons SO_2(1)$, $H_2O + SO_2(1) \rightleftharpoons H^+ + HSO_3^-$. The effective Henry's law constant for this case is $H^* \equiv (n_{tot}k_BT)/p = (n_{SO_2(l)} + n_{HSO_3^-})(k_BT/p) = H_0 + (KH_0k_BT/p)^{1/2}$, where n_{tot} is the number density of all sulfur-containing molecules in the bulk, $K \equiv n_{HSO_3^-}n_{H+}/n_{SO_2(l)} \simeq n_{HSO_3^-}^2/n_{SO_2(l)}$ is the dissociation constant, and H_0 is the molecular Henry's law constant. In bulk liquid, when SO_2 dissociates and controls the solution pH, $n_{tot} = H^*p \propto p^{1/2}$. If we assume the diffusivity to be independent of the pressure, we find $H^*D^{1/2} \propto p^{-1/2}$. Hence, for a dissociating species $\tau(t)$ is a function of p. Equation [A.4] does not strictly apply in this case, but direct integration of Eq. [A.1] yields

$$p_{out}(t) = p_{in}\left(1 - \frac{L}{v}\frac{A_{ice}^{eff}}{2V_{air}}\sqrt{\frac{KH_0Dk_BT}{p_{in}\pi t}}\right)^2 \quad [A.7]$$

This equation is valid for $p/\tau(t) \gg |\partial p/\partial t|$. Since $p_{in}/p_{out} > 0.6$ for all but the shortest times, Eqs. [A.6] and [A.7] coincide within a few percent for $H^* = (KH_0k_BT/p_{in})^{1/2}$. Hence, whereas dissociation of the dissolving species does not change the functional form of the uptake kinetics, it does lead to a pressure dependence of the form $H^*D^{1/2} \propto p^{1/2}$, which strongly affects the total amount of trace gas uptake. For simplicity and without loss in accuracy we use Eq. [A.6] in our treatment of the packed ice beds (Eq. [1]) and apply the $p^{-1/2}$ dependence in H^* in order to take dissociation into account. Therefore, for all but the first moments during the uptake, Eqs. [A.6] and [A.7] coincide for a nondissociating species with $H^* = H_0$ and a dissociating species with $H^* = (KH_0k_BTp_{in})^{1/2}$.

A.2. Adsorption/Desorption Kinetics

Nondissociating species. In order to find the flux j to the surface in this case, we solve the adsorption equation $dN_s/dt = k_ap(N_t - N_s) - k_dN_s$, where N_s is the number of molecules per surface area of the adsorbing species, N_t the total number of sites, and k_a and k_d are adsorption and desorption constants (in units s^{-1} atm^{-1} and s^{-1}, respectively). From the solution of the differential equation for N_s we find the net flux of molecules to the surface, $j = dN_s/dt$, and a characteristic time $\tau(t) = V_{air}/(A_{ice}^{eff}k_aN_tk_BT)\exp[(k_ap + k_d)t]$. Note that τ is independent of x and p for small coverages of the trace gas on ice ($k_ap/k_d \ll 1$). Hence, for submonolayer adsorption/desorption we obtain from Eq. [A.5]

$$p_{out}(t) = p_{in}\exp\left(-\frac{L}{v}\frac{A_{ice}^{eff}k_aN_tk_BT}{V_{air}}e^{-k_dt}\right). \quad [A.8]$$

Dissociating species. If the adsorbing species dissociates on the surface, the adsorption equation reads $dN_s/dt = k_ap(N_t - N_s) - k_d'n_s^2$. For small coverages ($N_s \ll N_t$), we find $\tau(t) = (V_{air}/k_BT A_{ice}^{eff}k_aN_t)\cosh^2((k_ak_d'pN_t)^{1/2}t)$. In this case, the solution of the flow tube equation involves an exponential integral and must be carried out numerically.

REFERENCES

1. Clapsaddle, C., and Lamb, D., *Geophys. Res. Lett.* **16,** 1173–1176 (1989).
2. Conklin, M. H., Laird, K., Sommerfeld, R. A., and Villinski, J. E., *Atmos. Environ. A* **27,** 159–166 (1993).
3. Dash, J. G., Fu, H., and Wettlaufer, J. S., *Rep. Prog. Phys.* **58,** 115–167 (1995).
4. Petrenko, V. F., and Whitworth, R. W., "Physics of Ice," Oxford Univ. Press, Oxford, 1999.
5. Hobbs, P. V., "Ice physics," Clarendon Press, Oxford, 1974.
6. Chen, J. P., and Crutzen, P. J., *J. Geophys. Res.* **99**(D9), 18847–18859 (1994).
7. Baker, M., and Nelson, J., *J. Geophys. Res.* **102**(D17), 23035–23038 (1996).
8. Knight, C. A., *J. Geophys. Res.* **101**(D8), 12933–12936 (1996).
9. Knight, C. A., *J. Geophys. Res.* **101**(D8), 12921–12928 (1996).
10. Baker, M. B., and Dash, J. G., *J. Geophys. Res.* **101**(D8), 12929–12931 (1996).
11. Tabazadeh, A., and Turco, R. P., *J. Geophys. Res.* **98**(D7), 12727–12740 (1993).
12. Wolff, E. W., and Mulvany, R., *Geophys. Res. Lett.* **18**(6), 1007–1010 (1991).
13. Kroes, G. J., and Clary, D. C., *J. Phys. Chem.* **96,** 7079–7088 (1992).
14. Abbat, J. P. D., and Molina, M. J., *J. Phys. Chem.* **96,** 7674–7679 (1992).
15. Carslaw, K. S., and Peter, Th., *Geophys. Res. Lett.* **24**(14), 1743–1746 (1997).
16. Thibert, E., and Dominé, F., *J. Phys. Chem.* **102,** 4432–4439 (1998).
17. Diehl, K., Mitra, S. K., and Pruppacher, H. R., *Atmos. Environ.* **29**(5), 975–981 (1995).
18. Peter, Th., *Annu. Phys. Chem.* **48,** 785–822 (1997).
19. Carslaw, K. C., Peter, Th., and Clegg, S. L., *Rev. Geophys.* **35**(2), 125–154 (1997).
20. Colbeck, S. C., *J. Colloid Interface Sci.* **72**(3), 371–384 (1979).
21. Nye, J. F., *J. Glaciol.* **37,** 401–413 (1991).
22. Mader, H., *J. Glaciol.* **38,** 359–374 (1992).
23. Mader, H., *J. Glaciol.* **38,** 333–347 (1992).
24. Keyser, L. F., and Leu, M. T., *J. Colloid Interface Sci.* **155,** 137–145 (1993).
25. Leu, M. T., Keyser, L. F., and Timonen, R. S., *J. Phys. Chem.* **101,** 6259–6262 (1997).
26. Golecki, I., and Jaccard, C., *Phys. Lett. A* **63,** 374–376 (1977).
27. Caranti, J. M., and Illingworth, A. J., *J. Phys. Chem.* **87,** 4078–4083 (1983).
28. Furukawa, Y., and Yamamoto, M., *J. Cryst. Growth* **82,** 665–677 (1987).
29. Mizuno, Y., and Hanafusa, N., *J. Phys.* **48**(C1), 511–517 (1987).
30. Elbaum, M., Lipson, S. G., and Dash J. G., *J. Cryst. Growth* **129,** 491–505 (1993).
31. Lied, A., Dosch, H., and Bilgram, J. H., *Physica B* **198,** 92–96 (1994).
32. Dosch, H., Lied, A., and Bilgram, J. H., *Surf. Sci.* **327,** 145–164 (1995).
33. Conklin, M. H., and Bales, R. C., *J. Geophys. Res.* **98,** 16851–16855 (1993).
34. Molina, M. J., *in* "Chemistry of the atmosphere: Its impact on global change" (J. G. Calvert, Ed.), pp. 27–38, Blackwell Sci., Oxford, 1994.
35. Thibert, E., and Dominé, F., *J. Phys. Chem.* **101,** 3554–3565 (1997).

36. Lelieveld, J., "C, N, P and S biogeochemical cycles," pp. 305–332, Springer Verlag, Berlin, 1992.

37. Seinfeld, J. H., "Atmospheric chemistry and physics of air pollution," Wiley-Interscience, New York, 1986.

38. Sommerfeld, R. A., and Lamb, D., *Geophys. Res. Lett.* **13,** 349–351 (1986).

39. Valdez, M. P., Dawson, G. A., and Bales, R. C., *J. Geophys. Res.* **44**(D1), 1096–1103 (1989).

40. Valdez, M. P., Bales, R. C., Stanley, D. A., and Dawson, G. A., *J. Geophys. Res.* **92**(D8), 9779–9787 (1987).

41. Mitra, S. K., Barth, S., and Pruppacher, H. R., *Atmos. Environ. A* **24**, 2307–2312 (1990).

42. Langenberg, S., and Schurath, U., *in* "Tropospheric oxidation mechanism: Temperature dependent trace gas–water interactions," European Commission, Luxemburg, 1995.

43. Langenberg, S., *Anwendung der Kapillar-Gaschromatographie zur Untersuchung von Spurengas-Aerosolwechselwirkungen*, Dissertation, Universität Bonn, 1997.

44. Gross, G. W., *J. Colloid. Interface Sci.* **25,** 270–279 (1967).

45. Ketcham, W. M., and Hobbs, P. V., *Philos. Mag.* **19,** 1161–1173 (1969).

46. Beaglehole, D., and Nason, D., *Surf. Sci.* **96,** 357–363 (1980).

47. Kouchi, A., Furukawa, Y., and Kuroda, T., *J. Phys.* **48**(C1), 676–677 (1987).

48. Wettlaufer, J. S., *Phys. Rev. Lett.* **83**(12), 2516–2519 (1999).

49. Mulvaney, R., Wolff, E. W., and Oates, K., *Nature* **331,** 247–249 (1988).

50. Fukazawa, H., Sugiyama, K., and Mae, S., *J. Phys. Chem.* 102(D2), 4794–4807 (1998).

51. Schick, M., and Shih, W. H., *Phys. Rev. B* **35,** 5030–5035 (1987).

52. Mantovani, S., Valeri, S., Loria, A., and del Pennino, U., *J. Chem. Phys.* **72**(2), 1077–1082 (1980).

53. Legrand, M., and Mayewski, P., *Rev. Geophys.* **35**(3), 219–243 (1997).

54. Pruppacher, H. R., and Klett, J. D., "Microphysics of clouds and precipitation," 2nd edition, D. Reidel, Dordrecht, 1997.

55. Voldner, E. C., Barrie, L. A., and Sirois, A., *Atmos. Environ.* **20**(11), 2101–2123 (1986).

56. Bales, R. C., Valdez, M. P., and Dawson, G., *J. Geophys. Res.* **92**(D8), 9789–9799 (1987).

57. Ganzeveld, L., Lelieveld, J., and Roelofs, G.-J., *J. Geophys. Res.* **103**(D5), 5679–5694 (1998).

58. Bronshteyn, V. L., and Chernov, A. A., *J. Cryst. Growth* **112,** 129–145 (1991).

59. Danckwerts, P. V., "Gas–liquid reactions," McGraw-Hill, New York, 1970.

60. Huthwelker, T., and Peter, Th., *J. Chem. Phys.* **105,** 1661–1667 (1996).

61. Hanson, D. R., and Ravishankara, A. R., *J. Phys. Chem.* **97,** 12309–12319 (1993).

62. Gmelin, J. F., "*Gmelin's Handbuch der anorganischen Chemie, Schwefel*," 8th edition, Volume Part B, No. 2, Schwefel," Verlag Chemie, Weinheim, 1960.

63. Huthwelker, T., "Experimente und Modellierung der Spurengasaufnahme in Eis," Dissertation, Universität Bonn, Cuvillier Verlag Göttingen (1999).